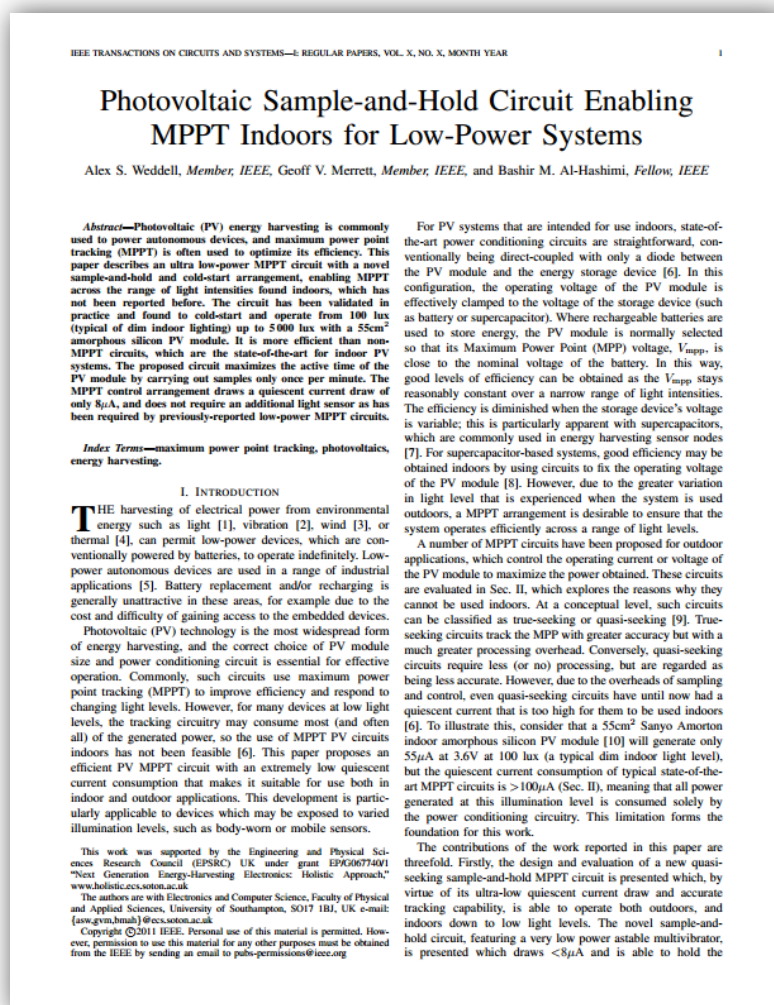


New paper now available with updated analysis and circuit design for photovoltaic energy harvesting

Thank you for your interest in our paper “An Efficient Indoor Photovoltaic Power Harvesting System for Energy-Aware Wireless Sensor Nodes.” If you are interested in this paper for the study of photovoltaic circuits for energy harvesting, we have recently published new and updated work on this which has been accepted for publication in IEEE Transactions on Circuits and Systems.

You can download this new paper from <http://eprints.soton.ac.uk/272832/>



Weddell, A., Merrett, G. and Al-Hashimi, B. (2011) Photovoltaic Sample-and-Hold Circuit Enabling MPPT Indoors for Low-Power Systems. *IEEE Transactions on Circuits and Systems I: Regular Papers* (In Press)

AN EFFICIENT INDOOR PHOTOVOLTAIC POWER HARVESTING SYSTEM FOR ENERGY-AWARE WIRELESS SENSOR NODES

A.S. Weddell*, N.R. Harris, N.M. White

Pervasive Systems Centre, School of Electronics and Computer Science, University of Southampton, UK

*Corresponding author: Tel: +44(0)23 8059 4996 Fax: +44(0)23 8059 2901 Email: asw05r@ecs.soton.ac.uk

Abstract: Wireless sensor nodes are autonomous devices which sense parameters and communicate them wirelessly. Their independent operation precludes the use of wired power supplies, and energy harvesting is becoming an attractive alternative to batteries. This paper presents the circuit design and embedded software of a photovoltaic power harvesting system for indoor wireless sensor nodes, which delivers energy-awareness and improved efficiency levels.

Keywords: photovoltaic energy harvesting, wireless sensor networks, energy management

INTRODUCTION

Wireless sensor nodes are autonomous devices which sense parameters and communicate them wirelessly (generally via radio protocols such as IEEE 802.11-2007 [1] or ZigBee [2]). As they operate without cabling, they must be self-sufficient for their energy provision. Conventionally, such devices are powered by non-rechargeable batteries, but recent advances in energy harvesting and storage technologies now mean that nodes can be designed to operate indefinitely from energy 'harvested' from their environment.

A common form of energy harvesting technology is from light via photovoltaic (PV) modules, but low indoor light levels mean that power tracking circuitry designed for outdoor use is often too power-hungry to operate indoors. Conventionally, indoor PV energy harvesting circuits will simply consist of a diode between the PV module and a battery or capacitor, which inhibits the reverse flow of energy from the store when the cell is not exposed to sufficient light [3]. This arrangement is particularly inefficient when charging a supercapacitor from empty, as in this situation the PV module is forced to operate far from its maximum power point (MPP) voltage.

In order for sensor nodes to function effectively, they must be protected against out-of-tolerance supply voltages and have an awareness of their energy status. Transceivers and microcontrollers used in wireless sensing applications will typically have a very low sleep current (around 1 μ A) but draw large "bursts" (of around 25mA) when active. For this reason, energy harvested indoors from PV modules and other devices, which is normally of the order of 1mA, must be 'buffered' in batteries or supercapacitors.

A photovoltaic energy conversion circuit has been reported in a previous publication by the authors [4]. This paper presents an extension to this work, which permits the nominal power of the module, and the light level to which the cell is exposed, to

be deduced from the open-circuit voltage of the PV module. We present the developments to the circuit and the embedded software, along with the theoretical work undertaken, to deliver this functionality on a Texas Instruments CC2431 system-on-chip microcontroller and transceiver.

Energy-aware network algorithms such as those proposed in [5] balance the importance of messages against the energy status of the node. With indoor PV energy harvesting, delivering this awareness, along with high efficiency, is non-trivial but has been achieved and is described in this paper. Circuit extensions to protect the node hardware against under- and over-voltage events have also been developed, and are described later.

PV MODULE CHARACTERISTICS

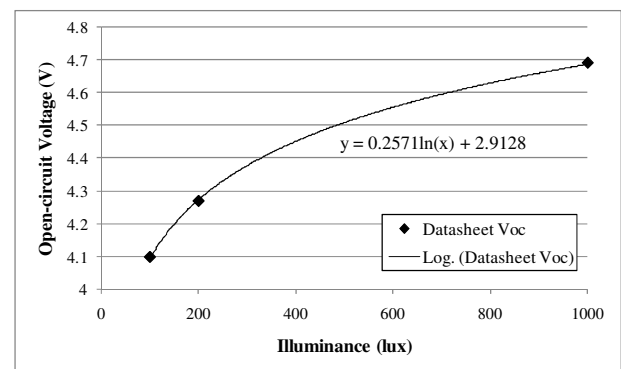


Figure 1. Logarithmic fit of V_{oc} against illuminance, for Schott Solar OEM 1116929 Indoor PV module.

Amorphous silicon (a-Si) photovoltaic cells have a relatively high efficiency at low light levels, compared to other types of cell. This makes them particularly suited to use indoors. The I-V characteristic of PV cells is described by the Shockley solar cell equation [3], and shown in (1). Here, k_B is the Boltzmann constant, T is absolute temperature, q is electronic charge, V is the voltage across the PV terminals, I_0 is the diode saturation current, and I_{ph} is the photogenerated current.

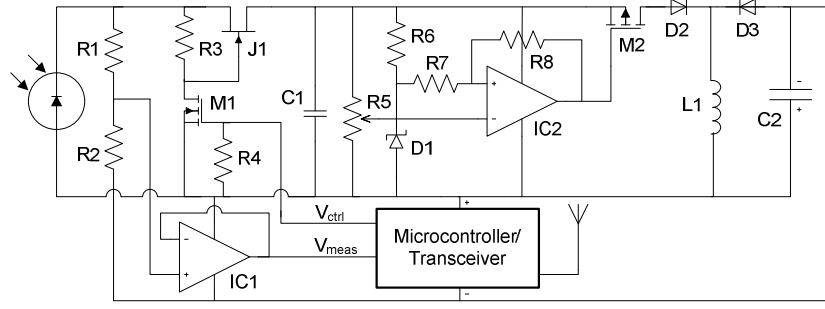


Figure 2. The developed photovoltaic energy harvesting circuit, which can be interrogated by the microcontroller.

$$I = I_{ph} - I_0 \left(e^{\frac{qV}{kBT}} - 1 \right) \quad (1)$$

The datasheet parameters for a Schott Solar OEM indoor solar cell [6] have been plotted and a logarithmic trend line has been added, as shown in Fig. 1. In this instance, the open-circuit voltage is approximated to the light level by equation (2).

$$V_{oc} = 0.2571 \ln(E_V) + 2.9128 \quad (2)$$

Where E_V is the illuminance level in lux, and can be generalized as equation (3), where A and B are parameters to be found for the individual PV module.

$$V_{oc} = A \ln(E_V) + B \quad (3)$$

This equation can be rearranged, as shown in (4), to determine the level of illuminance from V_{oc} .

$$E_V = e^{\frac{V_{oc}-B}{A}} \quad (4)$$

A useful property of silicon PV cells is that their MPP voltage (V_{mpp}) is related to their V_{oc} by parameter k . This parameter is typically between 0.70 and 0.80 (5), and can be determined for individual modules [3]. This property can be used by simpler maximum power point tracking circuits. Furthermore, the current obtained from the PV module at its MPP (I_{mpp}) is related to its illuminance by parameter m , as shown in (6).

$$V_{mpp} = kV_{oc} \quad (5)$$

$$I_{mpp} = mE_V \quad (6)$$

Table 1. Parameters found for Schott Solar OEM 1116929 Indoor PV Module.

Parameter	Description	Value
k	Ratio between V_{oc} and V_{mpp}	0.71
m	Ratio between E_V and I_{mpp}	5.4×10^{-7}
A	Natural log fit of $V_{oc}-E_V$	0.2571
B	Natural log fit of $V_{oc}-E_V$	2.9128

The nominal power (P_{nom}) obtained from the PV module can be estimated by means of (7), which makes use of the parameters outlined above and summarized in Table 1.

$$P_{nom} = V_{mpp} I_{mpp} = (V_{oc} \cdot k) \left(e^{\frac{V_{oc}-B}{A}} \cdot m \right) \quad (7)$$

There are certain limitations to this model, in that the parameter k only holds if the module is under uniform illumination (i.e. no partial shadowing). Secondly, parameter m holds only for relatively low levels of current. While it varies by less than 1% in the range 100-1000 lux, it can be expected to vary more widely in brighter deployment environments. However, the situation of interest to this investigation (indoor, artificially-lit environments) means that this simplification is acceptable. Lastly, the equation for nominal power assumes that the cell is operated at its maximum power point and the conversion circuitry is 100% efficient. The following section gives an idea of the efficiency of the circuit and other complications, but the result given for nominal power should be sufficient to give an idea of the energy harvesting status of the node, for use by energy-aware algorithms.

For SPICE simulation of the power conditioning circuit, a model was developed for the PV module used in this investigation. This was adapted from [7], and is shown in Fig. 3.

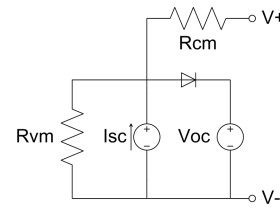


Figure 3. SPICE model for Schott Solar OEM 1116929 Indoor PV Module.

CIRCUIT DESIGN AND OPERATION

A circuit for indoor PV energy harvesting has been developed (Fig. 2), which consists of a modified buck-boost converter circuit with additional isolation and metrology circuitry. During normal operation, this circuit acts to maintain a constant voltage across its *input* terminals in order to keep the photovoltaic module at a voltage set by R4. The

photovoltaic module is maintained at this fixed voltage (in the range of maximum power point voltages of the cell at expected light levels) in order to keep its operation near its indoor MPP voltage. This simplification is acceptable as the normal range of indoor light levels is 100-1000 lux and in this range the power loss due to voltage clamping has been determined to be less than 3%.

The combination of JFET J1 and MOSFET M1 act to disconnect the load from the photovoltaic module when a 'high' signal is raised on the V_{ctrl} line. This permits the open-circuit voltage (V_{oc}) of the cell to be measured. However, a complication of this circuit is that, as it is based on a buck-boost converter, the input and output stages do not share a common ground (effectively the ground of the input is the V_{cc} of the output). For this reason, a high-impedance resistor divider comprised R1 and R2 is used to bring the V_{oc} signal into the range which can be interpreted by the microcontroller. The output from this divider is fed through a unity gain buffer around IC1 to provide the required low-impedance input to the ADC of the microcontroller. Resistors R3 and R4 act to ensure that the circuit operates normally on start-up, when supercapacitor C2 has built up insufficient voltage for the microcontroller to become active, and the switching converter is required to operate normally.

The V_{oc} of the module can be calculated by means of (8), where A is the ratio of R1 to R2, and $V_{\mu c}$ is the voltage at which the microcontroller is operating (i.e. the voltage across supercapacitor C2).

$$V_{oc} = (V_{meas} \times (A + 1)) - V_{\mu c} \quad (8)$$

R6 and D1 provide a reference voltage input to the micropower comparator IC2. R7 and R8 provide hysteresis to the system. In normal operation (when V_{ctrl} is low), C1 acts as a small buffer capacitor. When the voltage across C1 exceeds the threshold set by R5, comparator IC2 gives a 'low' output which switches MOSFET M2 'on' and permits current to flow through D2 and L1. After a very short period, the voltage across C1 will have dropped sufficiently to cause IC2 to turn M2 'off', and for energy to be transferred from L1 through D3 to be stored in supercapacitor C2 (note the polarity of this component).

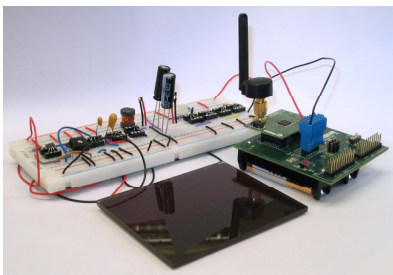


Figure 4. Photograph of the developed system.

SPICE simulations indicate that this circuit runs at over 70% efficiency with the PV module described earlier under normal indoor lighting. Although the absolute efficiency of the circuit has not been tested, practical tests comparing the circuit shown in Fig. 4 against a conventional diode-only system show a 30% improvement in node start-up times under normal office lighting.

The voltage on supercapacitor C2 is monitored by the microcontroller to determine the energy stored, and used to estimate its remaining lifetime.

Additionally, not shown in Fig. 2, is under- and over-voltage protection circuitry. This is important in wireless sensor node applications as under-voltage events can cause the microcontroller to turn on erroneously in an undefined state and drain power from the store, and overvoltage situations can cause permanent damage to the node. Over- and under-voltage protection circuitry has been implemented with the aid of voltage detector ICs.

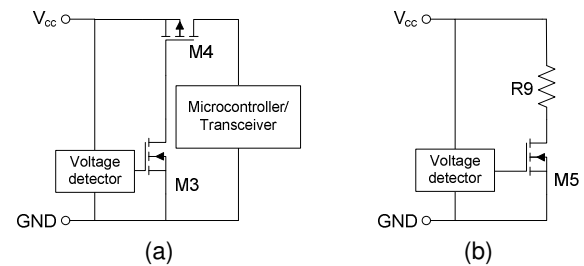


Figure 5. Under-voltage and over-voltage protection circuits, as implemented in demonstration system.

As shown in Fig. 5(a), a 2.0V voltage detector IC feeds through to digital MOSFETs M3 and M4 which interrupt the supply connection of the microcontroller, should the input voltage fall below 2.0V. The voltage detector has built-in hysteresis to mitigate issues with repeated switching. Overvoltage protection can be implemented in two ways: the system implemented in the demonstrator is shown in Fig. 5(b), in which a 3.3V voltage detector turns on a digital MOSFET which drains excess current through R9 when the threshold is crossed. Alternatively, it would be equally feasible for the output from this detector to be fed back to the V_{meas} input of the circuit in Fig. 2, thus disconnecting the cell and preventing further energy from being switched through.

EMBEDDED SOFTWARE DESIGN

The embedded software of the sensor node incorporates an "energy stack", a concept introduced in [8] and shown in Fig. 6 as part of a unified stack. This abstracts the energy management functions of the node in order to promote modularity and adaptability. The physical functions to 'interrogate' the photovoltaic module and obtain a raw voltage reading are implemented in the "physical energy" layer. The "energy analysis" layer hosts the mathematical functions

that which allow an estimate of the energy resource to be calculated. The “energy control” layer processes requests for data from the application, and presents the results to it in a standard fashion.

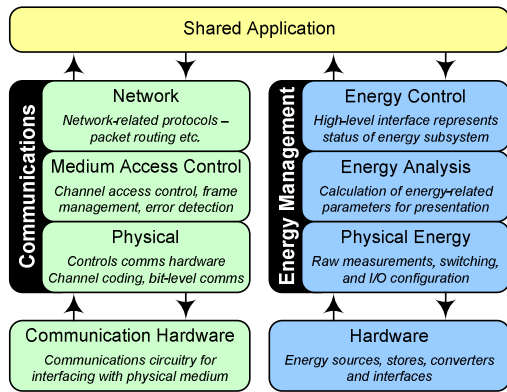


Figure 6. Energy and sensing stacks, as implemented in the demonstrator system.

In order to determine P_{nom} , it is necessary to use the equation given at (1). The Taylor series expansion for e^x is given by (9), which simplifies to (10). Taylor expansions are suitable for implementation in microcontrollers as they provide relatively simple approximations for a range of mathematical functions.

$$e^x = 1 + \frac{x^1}{1!} + \frac{x^2}{2!} + \frac{x^3}{3!} + \frac{x^4}{4!} + \dots \quad (9)$$

$$e^x = 1 + x + \frac{x^2}{2} + \frac{x^3}{6} + \frac{x^4}{24} + \dots \quad (10)$$

The function for e^x implemented in our 8-bit microcontroller calculates its value up to 10 terms. The accuracy and effectiveness of the function is limited firstly by the maximum size of long integers (32 bits, thus giving a limit of 12!, or 12 terms), and secondly by the precision of floating-point numbers (also 32 bits) and their operations, meaning that accuracy is potentially lost at each iteration.

The final component in the system is a balancing algorithm which controls message transmission dependent on the calculated energy status. This allocates a “power priority” to the status of the energy subsystem, meaning that the application layer can make high-level decisions without a detailed knowledge of the circuitry.

The system has been tested and evaluated in an office environment with a mix of natural and fluorescent lighting. From cold-starting, the system steadily charged the supercapacitor energy store C2 until the system voltage reached approximately 2.1V, at which point the microcontroller became active and started transmitting with a 30s sleep period. At its peak level of harvesting the system reported a nominal power level of 3.5mW, but a more typical level was around 1mW.

As the voltage across C2 increased, the sleep period of the system decreased in steps, until it was reporting its parameters every 1s. When the system voltage reached 3.45V, the overvoltage protection circuit was observed to restrict the voltage to between 3.35-3.45V.

CONCLUSIONS

An efficient circuit for harvesting energy indoors from a PV module has been demonstrated. The circuit permits the open-circuit voltage of the PV module to be determined by a simple 8-bit microcontroller, which is then transmitted via a 2.4GHz ISM band transceiver. The system is completely self-powered, and incorporates under- and over-voltage protection circuitry to regulate the operation of the sensor node.

The performance of the PV module has been modeled and an algorithm to determine the nominal power of the module from its V_{oc} has been developed, implemented, and tested. Limitations to the scheme have been described, but have a minimal impact on the indoor deployment scenario described in this paper. The system analyses the energy stored on the supercapacitor and uses this to determine its reporting frequency. This work forms part of a complete scheme for the energy-aware operation of wireless sensor nodes harvesting energy from their indoor environment.

ACKNOWLEDGEMENTS

The work reported on in this paper was undertaken as part of the Data Information Fusion Defence Technology Centre (DIF DTC) Phase II ‘Adaptive Energy-Aware Sensor Networks’ project, funded jointly by the UK Ministry of Defence and General Dynamics UK.

REFERENCES

1. IEEE Standards Association, *IEEE Std 802.11-2007*, New York, 2007.
2. ZigBee Standards Organization, *ZigBee Specification*, San Ramon, 2008.
3. T. Markvart, editor; *Practical Handbook of Photovoltaics: Fundamentals and Applications*, Oxford 2006.
4. A.S. Weddell, G.V. Merrett, N.R. Harris, B.M. Al-Hashimi, *Measurement+Control*, 41(4) pp. 104-108.
5. G.V. Merrett, N.R. Harris, B.M. Al-Hashimi, N.M. White; *Sensors and Actuators A: Physical*, 142 (2008), pp 379-389.
6. Schott Solar GmbH, *ASI@-OEM Solarmodules for Indoor*, Putzbrunn, 2006.
7. S.G. Hageman, *Electronics Design News*, May 1992, pp. 220.
8. G.V. Merrett, A.S. Weddell, N.R. Harris, B.M. Al-Hashimi, N.M. White, “A Structured Hardware/Software Architecture for Embedded Sensor Nodes”, *Proc. ICCCN 2008* (in press).